Environmental Science
Water Research & Technology

Elimination of transforming activity and gene degradation during UV and UV/H_2O_2 treatment of plasmid-encoded antibiotic resistance genes

Journal:	*Environmental Science: Water Research & Technology*
Manuscript ID	EW-ART-03-2018-000200.R2
Article Type:	Paper
Date Submitted by the Author:	27-May-2018
Complete List of Authors:	Yoon, Younggun; Gwangju Institute of Science and Technology, School of Earth Sciences and Environmental Engineering Dodd, Michael; University of Washington, Civil and Environmental Engineering Lee, Yunho; Gwangju Institute of Science and Technology, Environmental Science and Engineering

Water Impact Statement

The efficiency and mode of actions for deactivating and degrading antibiotic resistance genes (ARGs) during water treatment with UV (254 nm) and UV/H_2O_2 have been poorly understood. Here, we show that efficiency of elimination of the transforming activity for a plasmid-encoded ARG during the UV-based treatments depends on the rate of formation of cyclobutane-pyrimidine dimers (CPDs) in the plasmid and the repair of such DNA damage during the transformation process in host cells. This work has important contributions to optimizing the monitoring and operation of UV-based water disinfection and oxidation processes for removing ARGs.

Elimination of transforming activity and gene degradation during UV and UV/H_2O_2 treatment of plasmid-encoded antibiotic resistance genes

Younggun Yoon[1], Michael C. Dodd[2], Yunho Lee[1]*

[1]School of Earth Sciences and Environmental Engineering, Gwangju Institute of Science and Technology (GIST), Gwangju 61005, Republic of Korea

[2]Department of Civil and Environmental Engineering, University of Washington, Seattle, WA 98195, USA

*Corresponding author: Yunho Lee; Phone: +82 62-715-2468; Fax: +82 62-715-2434; Email: yhlee42@gist.ac.kr

Submitted to Environmental Science: Water Research & Technology

Abstract

To better understand the elimination of transforming activity of antibiotic resistance genes (ARGs), this study determined deactivation of transforming activity of an ARG (in *Escherichia coli* as a host) and the ARG degradation (according to quantitative PCR [qPCR] with different amplicon sizes) during UV (254 nm) and UV/H_2O_2 treatment of plasmid pUC19 containing an ampicillin resistance gene (amp^R). The required UV fluence for each $\log_{10}$ reduction of the transforming activity during UV treatment was ~37 mJ/cm^2 for both extra- and intra-cellular pUC19 (the latter within *E. coli*). The resulting fluence-based rate constant (k) of ~6.2×10^{-2} cm^2/mJ was comparable to the k determined previously for transforming activity loss of plasmids using host cells capable of DNA repair, but much lower (~10-fold) than that for DNA repair–deficient cells. The k value for pUC19 transforming activity loss was similarly much lower than the k calculated for cyclobutane-pyrimidine dimer (CPD) formation in the entire plasmid. These results indicate a significant role of CPD repair in the host cells. The degradation rate constants (k) of amp^R measured by qPCR increased with the increasing target amplicon size (192–851 bp) and were close to the k calculated for the CPD formation in the given amplicons. Further analysis of the degradation kinetics of plasmid-encoded genes from this study and from the literature revealed that qPCR detected most UV-induced DNA damage. In the extracellular plasmid, DNA damage mechanisms other than CPD formation (e.g., base oxidation) were detectable by qPCR and gel electrophoresis, especially during UV/H_2O_2 treatment. Nevertheless, the enhanced DNA damage for the extracellular plasmids did not result in faster elimination of the transforming activity. Our results indicate that calculated CPD formation rates and qPCR analyses are useful for predicting and/or measuring the rate of DNA damage and predicting the efficiency of transforming activity elimination for plasmid-encoded ARGs during UV-based water disinfection and oxidation processes.

Keywords: antibiotic resistance, ampicillin resistance gene, qPCR, transforming activity, UV, cyclobutane-pyrimidine dimer

Introduction

Increasing antibiotic resistance is a major threat to human and animal health, as it can lower the therapeutic potential of antibiotics against bacterial infections (WHO, 2014). Although antibiotic resistance can occur naturally, overuse or misuse of antibiotics in modern society is associated with increased antibiotic resistance (Allen et al., 2010). Antibiotics can select antibiotic-resistant bacteria (ARB) that carry genes (ARGs) responsible for antibiotic resistance mechanisms. The presence of ARB and ARGs in aquatic environments is a concern because it can promote the spread of antibiotic resistance through natural and anthropogenic water cycles (Berendonk et al., 2015; Pruden, 2014). In addition, antibiotic resistance can be disseminated among bacterial populations by sharing (mobile) ARGs through horizontal gene transfer (HGT) processes (Thomas and Nielsen, 2005). To minimize dissemination of environmental sources of antibiotic resistance, the necessity of coordinated national and international strategies has been advised for monitoring, risk assessment, and mitigation of antibiotic resistance (Vikesland et al., 2017).

Municipal wastewater has been identified as one of the hotspots that release ARB and ARGs into aquatic environments (Rizzo et al., 2013; Tan and Shuai, 2015). Conventional wastewater treatment does not fully eliminate ARB and ARGs (Chen and Zhang, 2013; Rizzo et al., 2013). Biological treatment processes (e.g., activation of sludge) can significantly reduce the load of ARB but may select highly (or multi-) resistant bacterial species (Czekalski et al., 2012). Disinfection of wastewater effluents with chlorine or ultraviolet irradiation (UV) has been widely practiced for water resource protection (Jacangelo and Trussell, 2002). Ozonation has recently received renewed attention as an option for treating municipal wastewater effluents to

eliminate organic micropollutants (Lee and von Gunten, 2016). Advanced oxidation processes such as UV/H_2O_2 treatment have also been tested to achieve the same goal (Gerrity et al., 2016; Miklos et al., 2018). There has been growing interest in the efficiency of wastewater disinfection and oxidation processes to lower the levels of ARB and ARGs, in addition to micropollutant elimination (Alexander et al., 2016; Czekalski et al., 2016; Dodd, 2012; Ferro et al., 2017; Lüddeke et al., 2015; McKinney and Pruden, 2012; Pak et al., 2016; Sousaa et al., 2017; Yoon et al., 2017).

ARGs in wastewaters exist in different forms such as intracellular (within bacteria) and extracellular, as free DNA and viruses (Colomer-Lluch et al., 2011; Zhang et al., 2018). ARGs can transfer resistance by HGT mechanisms such as conjugation, transduction, and transformation. Among these HGT mechanisms, transformation requires only intact ARGs for the resistance transfer, as extracellular ARGs can be taken up and incorporated into the genomes of competent bacteria even in the absence of the original donor ARB cell (Thomas and Nielsen, 2005). This mechanism is therefore different from conjugation or transduction in which viable donor cells or infective viruses containing ARGs are needed. Considering the potential for ARG transfer via transformation, it is necessary to assess the efficiency of disinfectants at destroying ARGs and eliminating their associated transforming activities (Dodd, 2012).

Molecular mechanisms of DNA damage induced by UV or by hydroxyl radicals ($^{\bullet}OH$) are well established. UV (particularly UVC) mainly generates DNA base lesions such as cyclobutane-pyrimidine dimers (CPDs) and pyrimidine (6-4) pyrimidone adducts [(6-4) photoproducts] (Görner, 1994; Sinha and Häder, 2002). Good correlations have been found between the UV-induced degradation rate of ARGs and the number of adjacent pyrimidine dimer sites (Chang et al., 2017; Destiani et al., 2017; McKinney and Pruden, 2012). Genomic modeling, an approach to predict the UV sensitivity of microorganisms based on their DNA sequence characteristics, has been tested to predict the degradation efficiency of ARGs

(Destiani et al., 2017). For $^{\bullet}$OH, the DNA damage can range from base oxidation to sugar backbone breakages, where the latter can lead to single strand (ss) and double strand (ds) breaks (von Sonntag, 2006). Despite this knowledge, it is unclear how different types of DNA damage resulting from reactions with disinfectants (e.g., UV, $^{\bullet}$OH) are related to the loss of ARG transforming activity.

Quantitative polymerase chain reaction (qPCR) has been widely used to detect and quantify ARGs present in aquatic environments (Luby et al., 2016). The qPCR method has also been employed to assess the efficacy of disinfection processes for ARG elimination by quantifying target qPCR amplicons (Alexander et al., 2016; Czekalski et al., 2016; Destiani et al., 2017; Ferro et al., 2017; Lüddeke et al., 2015; McKinney and Pruden, 2012; Pak et al., 2016; Sousaa et al., 2017; Yoon et al., 2017). Most qPCR methods involve amplicons covering only portions of ARGs (e.g., 100–200 bp) and rarely cover the entire genes that are necessary for gene transfer pathways (Chang et al., 2017; McKinney and Pruden, 2012; Yoon et al., 2017). In addition, the sensitivity of qPCR and bacterial gene transformation to DNA damage can differ due to the different degree of DNA repair or DNA polymerase fidelity rates of qPCR vs. the bacterial cell system (Chang et al., 2017). As an alternative approach, the transforming activity of ARGs can be directly measured by transformation assays in which the target ARG-containing DNA (e.g., plasmid) is taken up by and incorporated into the genomes of nonresistant, competent bacterial cells (Dodd, 2012; Luby et al., 2016). Nevertheless, few studies have applied such an ARG transformation assay to assess the efficacy of disinfection processes for the elimination of antibiotic resistance (Chang et al., 2017). Furthermore, the relationship between the qPCR method and the transformation assay for determining a biologically active ARG concentration is still poorly understood.

To elucidate the efficiency of deactivation and degradation of ARGs during water disinfection and oxidation processes, in this study, we determined and compared the changes in

transforming activity and ARG concentrations during UV_{254nm} (hereafter UV) or UV/H_2O_2 treatment of plasmid-encoded ARGs in bench scale disinfection experiments. A quantitative transformation assay employing *Escherichia coli* as the recipient was conducted to determine the transforming activity of the target plasmid. ARG concentrations were determined by qPCR with different amplicon sizes to determine the DNA damage in different parts of the target plasmid. In addition, agarose gel electrophoresis was carried out to determine structural changes of the plasmid. Both extracellular and intracellular forms of plasmids were treated to test the effects of cellular components on the efficiency of ARG elimination. The results were evaluated with respect to factors affecting the efficiency of elimination of ARGs' transforming activities; for example, DNA repair, plasmid characteristics, the type of DNA damage, and sensitivity of DNA polymerase.

Materials and Methods

Standards and reagents

All chemicals and solvents (mostly of ≥95% purity) were purchased from various commercial suppliers and used as received (SI-Text-1). Chemical solutions were prepared with ultrapure water (≥18.2 MΩ·cm) that was obtained by means of a Barnstead purification system (Thermo Fisher Scientific, USA). Glassware was washed with ultrapure water and autoclaved at 121°C for 15 min prior to use.

Model bacterial strains and ARG-containing plasmid

E. coli DH5α hosting plasmid pUC19 served as the model ARB in this study (Casali and Preston, 2003). Nonresistant *E. coli* DH5α was used as the recipient strain for the ARG transformation assay. The *E. coli* stocks were prepared at concentrations of ~10^9 colony-forming units (CFU)/ml according to the method described elsewhere (Yoon et al., 2017). Cells

144 from the midexponential growth phase were used. Plasmid pUC19 (2686 bp) is an *E. coli* vector
145 that carries an ampicillin resistance gene (amp^R; see Figure S1 and Table S1 for gene
146 information). Plasmids were extracted from *E. coli* stocks with the AccuPrep Nano-Plus
147 Plasmid Extraction Kit (Bioneer, 2016). Extracted plasmids were analyzed and quantified on a
148 NanoDrop ND-2000 spectrophotometer (NanoDrop Products, Wilmington, USA). Plasmid
149 concentrations in the extracted stock solutions (50 μL) were ~10^{11} copies/μL (or 0.5–1 μg/μL).
150 See SI-Text-2 for further details.

151 **Determination of transforming activity of plasmid-encoded ARG**

152 To quantify the ability of the pUC19 plasmid to transfer its antibiotic resistance, a
153 transformation assay was conducted with nonresistant *E. coli* DH5α as the recipient strain
154 (Hanahan, 1983). Competent cells were prepared by treating *E. coli* DH5α with calcium
155 chloride and glycerol as the chemical treatment method (Shanehbandi et al., 2013) and stored at
156 -80°C until use (see SI-Text-3 for details). One-hundred μL of the competent cells (~7×10^8
157 CFU/ml) was thawed and prepared in 1.5 mL tubes, and mixed with 5–10 μL of the plasmid
158 samples. The resulting mixtures were placed on ice for 30 min incubation, then quickly
159 transferred into a water bath at 42°C for 45 s and placed back on ice for 2 min. After heat shock,
160 the samples were mixed with 900 μL of Luria-Bertani (LB) broth and cultured in a shaking
161 incubator (200 rpm) at 37°C for 45 min. The incubated samples were serially diluted with LB
162 broth and plated onto LB agar plates containing 50 mg/L ampicillin. The concentration of the
163 transformants was determined by enumerating the ARB colonies on the plates after 24 hours of
164 incubation in the dark at 37°C. Finally, the transforming activity of the samples was calculated
165 as the concentration of transformants from colonies in selective plates (with ampicillin)
166 normalized to the concentration of *E. coli* cells from colonies in nonselective plates (without

ampicillin) as presented in Eq. 1. From the nonselective plates, typical concentrations of ~7 × 10^8 CFU/mL *E. coli* cells were determined under the tested conditions.

$$\text{Transforming activity} = [\text{Transformants}]_{\text{selective plate}} \div [\textit{E. coli}\ \text{cells}]_{\text{nonselective plate}} \quad [1]$$

qPCR

Amplicons spanning variable-length segments of the amp^R gene (192, 400, 603, and 851 bp of the overall 861 bp length of amp^R) and *ori* region (190, 390, and 530 bp of the overall 589 bp length of *ori*) in the pUC19 plasmid (2686 bp) were quantified by means of qPCR (Figure S1, Table S1). Amplicon and primer sequences were determined from the pUC19 sequence retrieved from the NCBI GenBank database. Primers were designed using the NCBI Primer-BLAST tool (Table S2). qPCR measurements were performed on a CFX96 Real-Time PCR detection system (Bio-Rad, Hercules, CA, USA) using SsoFast™ EvaGreen® Supermixes (Bio-Rad). Standard curves were generated from 10-fold serial dilutions covering 5 orders of magnitude. Each 20 µL qPCR reaction consisted of 1 µL of 0.5 pmol forward and reverse primers (0.5 pmol/µl), 1 µL of a DNA sample, 10 µL of an EvaGreen® Supermix, and 8 µL of autoclaved DNase-free water. The temperature profile of the PCR protocol included one cycle at 95°C for 2 min; 30 cycles at 95°C for 5 s, an annealing step at 55°C for 60 s, and an extension step at 72°C for 20 s; followed by a melt curve analysis from 65°C to 95°C. The same PCR protocol was used for all qPCR assays with different amplicons. Calibration curves for the target amplicons exhibited r^2 values of ≥0.98 for all cases (Figure S2 shows a representative example). The average amplification efficiencies for the amp^R amplicons were 0.90(±0.04) for 192 bp, 0.89(±0.06) for 400 bp, 0.84(±0.09) for 603 bp, and 0.88(±0.08) for the 851 bp amplicon. The average amplification efficiencies for the *ori* amplicons were 0.84(±0.05) for 190 bp, 0.95(±0.03) for 390 bp, and 0.93(±0.07) for the 530 bp amplicon. The limit of detection (LOD) and quantification (LOQ) were determined as 15 copies and 40 copies per reaction for

most qPCR runs. The end products of qPCR analyses were also analyzed by agarose gel electrophoresis (Figure S3) to confirm successful amplification of the target genes. The samples from UV treatment were directly analyzed by the qPCR protocol described above for extracellular plasmids. For intracellular plasmids, 10 mL of a given sample containing disinfectant-treated or untreated *E. coli* DH5α cells was centrifuged, and the pellet was resuspended in 100 μL of Tris-HCl buffer (10 mM, pH 8.5). The resulting concentrated samples were processed with the AccuPrep Nano-Plus Plasmid Extraction Kit (Bioneer, 2016) and subsequently analyzed by the above qPCR protocol.

Gel electrophoresis

Samples were prepared by treating the extracted pUC19 (~5 μg/mL) at pH 7 (2 mM phosphate buffered solutions) with UV and UV/H_2O_2 at different UV fluence levels (0–312 mJ/cm^2). Linearized pUC19 plasmids were prepared by incubating the extracted pUC19 with type II restriction enzyme *EcoR*I (NEB, USA) at 37°C for 1 h, followed by enzyme inactivation at 65°C for 20 min. Standards of the *amp*^{R} amplicons with different sizes (192, 400, 603, and 851 bp) were prepared by qPCR reactions above. These prepared plasmid samples and a 1 kb DNA ladder (Enzynomics, KOREA) were loaded on 0.8% agarose gels containing 0.5 μg/ml ethidium bromide in 1× TAE (Tris-Acetate-EDTA) buffer and were separated at 4 V/cm for 35 min. Gel images were captured on a bench-top UV Transilluminator (Universal mutation detection system, UVP, LLC, USA). The density of each band on the gels was calculated by quantitative band analysis in the ImageJ software (Schneider et al., 2012). Isolated *amp*^{R} amplicons for the transforming activity determination were prepared by cutting the gels loaded with the *amp*^{R} qPCR amplicon mixtures and by subsequent purification with the AccuPrep® Gel Purification Kit (Bioneer).

UV and UV/H_2O_2 treatments

Bench scale UV irradiation experiments were conducted in a quasi-collimated beam system (Bolton and Linden, 2003) equipped with a low-pressure mercury lamp emitting 254 nm light (Sankyo Denki Ltd., Tokyo, Japan). The applied photon fluence rate was ~0.3 mW/cm^2 as determined by a UVX digital radiometer (Ultra-Violet Products Ltd., Upland, USA) or by atrazine chemical actinometry (Lee et al., 2016). Solutions of the pUC19 plasmid or *E. coli* were separately prepared in 2 mM phosphate buffer (pH 7) by adding the corresponding stock solutions at the concentration of ~10^{11} copies/mL for the plasmid or ~5×10^6 CFU/mL for *E. coli*, respectively. These samples (120 mL) were placed in a Petri dish reactor with a sample depth of 2.5 cm and were irradiated with UV light under gentle stirring using a magnetic stir bar. For UV/H_2O_2 experiments, 10 mg/L H_2O_2 was added to the samples before the UV irradiation. The absorbance of the samples was ≤ 0.02 cm^{-1} at 254 nm and the light screening (attenuation) coefficient in the Petri dish reactor was calculated to be ≥ 0.94 (Bolton and Linden, 2003). The presence of 10 mg/L of H_2O_2 alone as the control experiment did not induce the gene degradation within 40 min of contact time (Yoon et al., 2017). The decrease of H_2O_2 by the UV photolysis was less than 10% of its initial concentration within the applied UV fluence range (0 – 300 mJ/cm^2). Thus, the degradation of pUC19 by OH radicals (formed from the UV photolysis of H_2O_2) was in a first-order condition throughout the UV irradiation. The reaction solution was sampled (and in the latter case, also supplemented with bovine catalase (40 μg/mL) to quench residual H_2O_2) and was then stored at –20°C for 10 days. Triplicate experiments were conducted for each condition, and average sample concentrations (amplicon copies, transforming activity, or viable cell counts) reported with one standard deviation.

Statistical analysis

Statistical analyses were conducted in GraphPad Prism 7 (http://www.graphpad.com/). UV fluence-based first-order rate constants determined from different sets of experiments were

compared by multiple linear regression analyses. The null hypothesis in these analyses was that the first-order rate constants were not significantly different, with $p < 0.05$ as the significance cutoff.

Results

Quantitative determination of the transforming activity of plasmid-encoded *amp*^{R}

Figure 1 shows that the concentration of transformants after the plasmid transformation increases in proportion to the pUC19 concentration, with a slope of 1.0 in a log–log scale plot. The measured transforming activity ranged from 3.1×10^{-8} to 1.6×10^{-4} for the pUC19 concentrations ranging from 10^{-5} to 5.0×10^{-2} μg/mL. This result indicates good capacity of the assay for quantitative determination of the transforming activity. A total of ~2×10^8 transformants were formed per μg of the plasmid. The observed transformation efficiency is comparable to that reported in the literature (i.e., 2×10^8 to 10^9 transformants/μg of plasmid DNA; Hanahan et al., 1991).

The transforming activity of pUC19 (2.5×10^{-2} μg/mL) after the digestion with the *EcoRI* restriction enzyme was found to be ~10^{-6}, which was lower than that of intact pUC19 by a factor of 80. *EcoRI* can linearize pUC19 by DNA cutting (Pingound and Jeltsch, 2001). Thus, dsDNA breaks created by *EcoRI*, even outside the *amp*^{R} gene (especially at restriction site 284, see Figure S1), can significantly reduce the ampicillin resistance transforming activity of pUC19. Our data are consistent with other studies showing that the transformation efficiency of plasmids can decrease by two or three orders of magnitude after digestion of the plasmids with various restriction enzymes (Chang et al., 2017; Palmen et al., 1993; Schulte-Frohlinde, 1987). The transforming activities of *amp*^{R} gene fragments in a range of amplicon sizes (192, 400, 603, and 851 bp, see Figure S1) were also determined. These *amp*^{R} gene fragments (prepared at 10^{11}

copies/mL) showed negligible transforming activity (lower by more than four orders of magnitude) as compared to pUC19 at the same molar concentrations. This finding indicates that not only amp^R but also the whole plasmid is required for the transformation of amp^R.

Elimination of transforming activity of plasmid-encoded amp^R

Figure 2 shows decreases in the amp^R transforming activity (stars) during UV or UV/H_2O_2 treatment of extracellular (i.e., extracted plasmid) or intracellular (i.e., plasmid within *E. coli*) pUC19 at pH 7. The initial transforming activities in these experiments were ~10^{-4} and the transformation activity of ~10^{-8} was the limit of quantification of the method; thus, a ~4 log reduction could be detected. Without UV and UV/H_2O_2 treatment, *E. coli* and pUC19 were stable for several hours in the phosphate buffer according to the control assays.

The elimination of transforming activity followed first-order kinetics with respect to UV fluence in all cases ($r^2 \geq 0.99$). The fluence-based first-order rate constants (k) for the transforming activity loss could be determined from the slopes of the linear plots (i.e., $k = 2.303 \times$ slope). The k values for intracellular pUC19 (i-ARG) were 6.2(±0.4) × 10^{-2} cm^2/mJ for UV treatment (Figure 2a) and 6.4(±0.4) × 10^{-2} cm^2/mJ for UV/H_2O_2 treatment (Figure 2b), and for extracellular pUC19 (e-ARG) were 6.1(±0.3) × 10^{-2} cm^2/mJ for UV (Figure 2c) and 7.3(±0.4) × 10^{-2} cm^2/mJ for UV/H_2O_2 treatment (Figure 2d), respectively. The data showed that the rates of elimination of the transforming activity were almost the same for all cases, with k of ~6.2 × 10^{-2} cm^2/mJ ($p < 0.001$), except for the e-ARG treatment with UV/H_2O_2 yielding a slightly higher (by a factor of 1.2) deactivation rate. At a UV fluence of 40 mJ/cm^2 (typical for water disinfection), the achieved elimination of the transforming activity was a 1.0 log reduction (1.3 log for UV_{254}/H_2O_2 treatment of e-ARG). To achieve more extensive elimination of the transforming activity such as a 4-log reduction, the required UV fluence was found to be 150 mJ/cm^2 (125 mJ/cm^2 for UV_{254}/H_2O_2 treatment of e-ARG).

287 **Degradation of pUC19 fragments (*amp*^{R} and *ori* portions) determined by qPCR**

288 Figure 2 also presents changes in the logarithmic relative concentrations of the suite of
289 variable-length *amp*^{R} amplicons measured by qPCR (i.e., 192, 400, 603, and 851 bp) during UV
290 and UV/H_2O_2 treatment of *E. coli* (i-*amp*^{R}) and pUC19 plasmid (e-*amp*^{R}), respectively. In all
291 cases, the depletion of *amp*^{R} genes followed first-order kinetics with respect to the UV fluence
292 ($r^2 \geq 0.99$). The *k* values determined for the gene damage are summarized in Table 1. The
293 following points from these kinetic data are noteworthy. First, the gene damage rates of *amp*^{R}
294 increase with the increasing qPCR amplicon size. This result can be explained by the increasing
295 number of target sites for UV (e.g., adjacent pyrimidine dimer sites) with the increasing gene
296 size. Second, the gene damage was slower or faster than the transforming activity loss
297 depending on the qPCR amplicon size. For example, the 192 bp gene fragment underwent much
298 slower degradation (by a factor of 2.9–4.0 based on relative *k*) as compared to the loss of
299 transforming activity. The degradation rates of the 400 and 603 bp gene fragments were higher
300 and closer to the rates of ARG deactivation (i.e., transforming activity elimination). The
301 degradation rates of the 851 bp gene fragment were higher by a factor of 1.1–2.5 as compared to
302 those of the transforming activity loss. These results highlight the need to better understand the
303 relation between the gene damage determined by the qPCR method and the elimination of
304 transforming activity of plasmid-encoded ARGs (further details will be discussed later). Third,
305 the gene damage rates of e-*amp*^{R} were higher than those of i-*amp*^{R} in both UV and UV/H_2O_2
306 treatments ($p < 0.05$), and the difference was greater for the UV/H_2O_2 treatment. The gene
307 damage rates of i-*amp*^{R} were quite similar between UV and UV/H_2O_2 treatment ($p = 0.47$ for
308 192 bp, $p = 0.13$ for 400 bp, $p = 0.50$ for 604 bp, and $p = 0.82$ for 851 bp), whereas the gene
309 damage rates of e-*amp*^{R} were considerably higher in UV/H_2O_2 than in UV treatment ($p < 0.05$).
310 These results indicated that $^{\bullet}OH$ from UV photolysis of H_2O_2 can contribute to the degradation
311 of extracellular genes, but the effect of $^{\bullet}OH$ on intracellular genes is effectively negligible

312 compared to the UV-induced direct gene damage. A similar result was reported in our previous
313 work, and was explained by complete scavenging of •OH by cell membrane or cytoplasmic
314 components before reaching i-ARG (Yoon et al., 2017).

315 In this study, the qPCR method was also applied to measure damage in the *ori* region
316 (Figure S1), for assessing DNA reactivity outside the amp^R gene in pUC19. Figure S4 shows
317 decreases in the logarithmic relative concentration of *ori* as measured by the qPCR method with
318 amplicon sizes of 190, 390, and 530 bp during UV and UV/H_2O_2 treatment of extracellular
319 pUC19. The reactivity and degradation patterns of e-*ori* were similar to those of e-amp^R when
320 considering their gene sizes (see the *k* values in Table 1).

321 **Structural damage to pUC19 measured by gel electrophoresis**

322 Figure 3a & 3b presents the images of agarose gel electrophoresis analyses of pUC19
323 (prepared at 5 μg/mL) before and after UV and UV/H_2O_2 treatment (UV fluence range of 0–312
324 mJ/cm^2). Intact pUC19 yielded a band corresponding to a size slightly larger than the 2-kb
325 molecular weight (MW) marker, and pUC19 treated within *EcoRI* showed a band corresponding
326 to a size slightly larger than the 3-kb MW marker. The observed band positions are consistent
327 with the size of pUC19 (i.e., 2686 bp) and the fact that plasmids typically exist in a supercoiled
328 form (i.e., intact pUC19), which migrates faster than the linear form (i.e., *EcoRI*-treated pUC19)
329 in an agarose gel because of their conformational difference. After the UV treatment, the band
330 position of pUC19 changed negligibly. In contrast, the band gradually moved upward with
331 increasing UV fluence during UV/H_2O_2 treatment, indicating the conformational change of
332 pUC19 from the supercoiled to linear form. On the basis of quantitative agarose gel image
333 analyses (Schneider et al., 2012), the degree of linearization of pUC19 was found to be less than
334 10% during the UV treatment but increased up to 93% during the UV/H_2O_2 treatment with an
335 increase in UV fluence up to 312 mJ/cm^2 (Figure S5). These results can be explained by the fact

that UV mainly induces damage to the DNA bases such as CPDs (Görner, 1994; Sinha and Häder, 2002) that is not detected in the agarose gel analysis. During UV/H_2O_2 treatment, $^{\bullet}OH$ is formed and reacts with not only DNA bases but also the sugar phosphate backbone; the latter reaction can cause significant DNA damage such as dsDNA breaks (von Sonntag, 2006) that are detectable by agarose gel analysis. Finally, the rates of the plasmid structural (conformational) change were compared to the rates of transforming activity loss during UV and UV/H_2O_2 treatment. Figure 3c shows that the transforming activity loss occurred much faster than the structural degradation of the plasmid during UV and UV/H_2O_2 treatment. This finding indicates that the UV-induced damage to DNA bases is mainly responsible for the elimination of the transforming activity of plasmid-encoded ARGs. A similar conclusion has been reached in other studies (Chang et al., 2017; Yoon et al., 2017).

Discussion

Effects of DNA repair and plasmid characteristics on the efficiency of elimination of transforming activity

The efficiency of elimination of pUC19's transforming activity during UV irradiation, determined in this study, can be compared with that in other studies, in which several different plasmids were treated with UV (254 nm) and transformed into several strains of *E. coli* mutants (Gurzadyan et al., 1993) or *Acinetobacter baylyi* (Chang et al., 2017) as host cells. Table 2 summarizes the *k* values for the elimination of transforming activity and corresponding information on the plasmids and host cells used in these studies. Note that these plasmids (pUC19, pTZ18R, pBR322, and pWH1266) all contain a β-lactamase resistance gene (either amp^R or $bla_{\text{TEM-1}}$). pBR322 and pWH1266 also contain a tetracycline resistance gene (*tetA*).

Data from previous work reveals that the efficiency of elimination of transforming activity is greatly influenced by the type of *E. coli* recipient strain. When *E. coli* AB2480 (a double-

mutant strain lacking both *uvrA* and *recA* genes) was used as a recipient strain, the *k* value for UV-induced elimination of transforming activity was 5.3×10^{-1} cm^2/mJ for pTZ18R and 6.7×10^{-1} cm^2/mJ for pBR322. These values are 22- and 15-fold larger than the *k* value for pTZ18R (2.4×10^{-2} cm^2/mJ) and pBR322 (4.4×10^{-2} cm^2/mJ) when *E. coli* AB1157 (wild-type strain) was used. Relatively low-to-intermediate levels of *k* were observed for pTZ18R when single-mutant *E. coli* AB1886 (deficient in *uvrA*, $k = 7.1 \times 10^{-2}$ cm^2/mJ) and *E. coli* AB2463 (deficient in *recA*, $k = 6.7 \times 10^{-2}$ cm^2/mJ) strains were tested (Gurzadyan et al., 1993). These results can be explained by the different levels of DNA repair ability of the host cells. *uvrA* is one of the *uvr* genes responsible for DNA repair through the nucleotide excision repair (NER) pathway (Kisker et al., 2013). The *recA* gene is involved in various types of homologous recombination and is essential for the repair and maintenance of DNA in prokaryotes (Lusetti and Cox, 2002). Thus, the DNA repair in double-mutant *E. coli* AB2480 was negligible and resulted in a highly efficient loss of plasmid transforming activity. In contrast, DNA repair was significant in the other *E. coli* strains (i.e., single-mutant and wild-type strains), resulting in much slower elimination of the transforming activity.

The *k* value determined here for UV-induced deactivation of pUC19 in *E. coli* DH5α ($= 6.1 \times 10^{-2}$ cm^2/mJ) is close to that for pTZ18R in the *E. coli* AB2463 strain ($= 6.7 \times 10^{-2}$ cm^2/mJ). Of note, both *E. coli* strains are deficient in the *recA* gene, and the sizes of the two plasmids are comparable (2686 bp for pUC19 and 2861 bp for pTZ18R, Table 2). The *k* value for pWH1266 and wild-type *A. baylyi* is 1.1×10^{-1} cm^2/mJ (Chang et al., 2017), which is larger than that for pTZ18R and pBR322 with wild-type *E. coli* by a factor of 4.6 and 2.5, respectively. Notably, the size of pWH1266 is larger than that of pTZ18R and pBR322 by a factor of 3.1 and 2.0, respectively. Larger plasmids will typically contain a greater number of potential DNA damage sites and would accordingly be expected to show a higher rate of UV-induced elimination of transforming activity.

The rate of pyrimidine dimer formation vs. elimination of transforming activity of the plasmid

CPDs and (6-4) photoproducts are known as the major types of UV-induced DNA damage (Cadet and Douki, 2018; Görner, 1994; Sinha and Häder, 2002). These DNA damages are readily formed at adjacent pyrimidine sites such as intrastrand thymine-thymine (TT), thymine-cytosine (TC), cytosine-thymine (CT), and cytosine-cytosine (CC) doublets. The formation of CPDs usually predominates over formation of (6-4) photoproducts. In addition, the TT site is the most photoreactive in terms of CPD formation among the bipyrimidine doublets (Douki and Cadet et al., 2001; Douki, 2006). For instance, the following quantum yields of CPD formation (in number of CPDs formed per number of photons absorbed by the entire target DNA) have been reported during UV_{254} irradiation of dsDNA under typical solution conditions; 0.66×10^{-3} : 0.23×10^{-3} : 0.10×10^{-3} : 0.02×10^{-3} for TT : TC : CT : CC (Douki, 2006). The TC site also shows high yield for (6-4) photoproduct with a quantum yield of 0.19×10^{-3} (Douki, 2006). In light of this, we attempted to analyze the relationship between the formation rate of CPDs as the major UV-induced DNA damage and consequent elimination of the transforming activity of plasmid pUC19.

The UV fluence-based formation rate constant of CPDs (k_{CPDs}, cm^2/mJ) in dsDNA can be written as Eq. 2:

$$k_{CPDs} = (2.303 \times \varepsilon \times \Phi_{CPDs}) \div U \quad [2]$$

where ε (M^{-1} cm^{-1}) is the molar absorption coefficient, Φ_{CPDs} (mol/Einstein) is the quantum efficiency of CPD formation, and U (= 4.72×10^5 J/Einstein) is the molar photon energy at 254 nm [Lee et al. (2016) and references therein]. The Φ_{CPDs} values reported for dsDNA show variations due to different ways of defining the quantum yield. A Φ_{CPDs} value of ~2.4×10^{-3} (Görner, 1994) or ~1.0×10^{-3} (Douki, 2006) was obtained by considering the number of CPDs

formed per photons absorbed by the entire target DNA (Douki, 2006). In this case (Approach I, $k_{CPDs\text{-}I}$), the ε value for the entire target DNA should be used. The ε value for all base pairs in a strand of dsDNA can be conveniently estimated as $\varepsilon_{bp} = \varepsilon_{sbp} \times$ (# of base pairs) in which ε_{sbp} is the average molar absorption coefficient of a single base pair (ε_{sbp} = 15,000 M^{-1} cm^{-1}, Tataurov et al., 2008), and "# of base pairs" is the total number of base pairs in a given DNA. Alternatively, the quantum yield could be defined based on the photons absorbed specifically by two adjacent pyrimidines. In the current study, we focused on photon absorbance by TT sites, as they are the most photoreactive for CPD formation amongst the four pyrimidine doublets TT, TC, CT, and CC, and also reported to be the most slowly repaired in human skin cells (Cadet and Douki, 2018). In the case of TT sites (Approach II, $k_{CPDs\text{-}II}$), a $\Phi_{CPDs,TT}$ value of ~2.0×10^{-2} has been reported (Douki et al., 2000; Patrick, 1977). The ε value for all TT sites within a strand of dsDNA can be calculated as $\varepsilon_{TT} = \varepsilon_{sTT,254} \times$ (#TT), where ε_{sTT} is the molar absorption coefficient of a single TT site (= 8,400 M^{-1} cm^{-1}; Patrick, 1977), and #TT is the number of TT sites in a given DNA. Using the two different definitions of Φ_{CPDs} described above, $k_{CPDs\text{-}I}$ and $k_{CPDs\text{-}II}$ can be calculated for plasmids as a function of the number of base pairs and TT sites, respectively.

Figure 4 and Figure S6 show a comparison of the calculated k_{CPDs} values (dashed lines) with the measured k values for the elimination of transforming activity (symbols) from this study (pUC19) and from the literature (pTZ18R, pBR322, and pWH1266) as a function of the number of (a) base pairs ($k_{CPDs\text{-}I}$) and (b) TT sites ($k_{CPDs\text{-}II}$) in the plasmids. In addition, a Φ_{CPDs}, TT-II value of 2.0×10^{-2} was for Figure 4b and Figure S6b. Notably, k_{CPDs} ($k_{CPDs\text{-}I}$ and $k_{CPDs\text{-}II}$) were close to k measured when double-mutant *E. coli* was used as a recipient (differences ranging from factors of 1 to 2.3). This finding indicates that in the double-mutant strain, most of the CPDs formed in the plasmids led to the elimination of transforming activity because the

CPDs were not repaired in the corresponding host cell. The k values obtained with single mutants and wild-type *E. coli* and *A. baylyi* strains were significantly lower than k_{CPDs} by factors ranging from 5 to 15 (indicated as the ratio of the slopes compared to k_{CPDs}, Figure 4). This result strongly suggests a significant role of CPD repair activity in these host cells. One alternative explanation for these trends may be that some DNA damages on the plasmid are located where they do not inhibit the plasmid transformation, which requires further investigation. Overall, good linear trends were found between the measured k values and the number of base pairs and TT sites in the plasmids. These trends can be explained by the fact that more CPDs are formed with increasing gene fragment size, or – more specifically – increasing number of potential pyrimidine dimer sites. The observed linear relation can be further tested in future studies by determining k for plasmids with different gene fragment sizes and compositions, and in host cells with different DNA repair abilities.

The rate of pyrimidine dimer formation vs. gene damage measured by qPCR

Figure 5 and Figure S7 depict the plots of the measured k values (symbols) for the degradation of target qPCR amplicons as a function of (a) the number of base pairs and (b) the number of TT sites in the genes. In addition, k values were compared with the $k_{CPDs\text{-}I}$ and $k_{CPDs\text{-}II}$ values of the target genes that could be calculated via Eq. 2 and the method described above ($\Phi_{CPDs\text{-}I}$ of 2.4×10^{-3} for Figure 5a, 1.0×10^{-3} for Figure S7a, and $\Phi_{CPDs,TT\text{-}II}$ of 2.0×10^{-2} for Figure 5b and Figure S7b). The k data from UV treatment of extracellular and intracellular plasmids as well as the k data from the UV/H_2O_2 treatment of intracellular plasmids (but not extracellular plasmids) from this study and from the literature were included in the plots (Table 1). The UV/H_2O_2 data for i-ARGs were included because the damage to intracellular genes during UV/H_2O_2 treatment was exclusively caused by UV, with little contribution from $^{\bullet}OH$. The k values for extracellular plasmids during UV/H_2O_2 treatment were not included because

458 they were much larger compared to those of UV treatment, indicating a significant contribution
459 of $^{\bullet}$OH reactions to extracellular gene damage.

460 The following points are noteworthy and follow from the results in Figure 5. First, the
461 intracellular genes (circles) show good linear relations with the numbers of base pairs and TT
462 sites (dashed lines, $r^2 = 0.93$ for both cases), whereas k values for the extracellular genes
463 (triangles) correlated relatively poorly with the numbers of base pairs and TT sites. Second, the
464 number of TT sites ($k = (6.4 \times 10^{-4}) \times$ (# of TT sites), $r^2 = 0.77$, n = 25) yielded a better linear
465 correlation with k as compared to the number of base pairs ($k = (8.9 \times 10^{-5}) \times$ (# of base pairs),
466 $r^2 = 0.65$, n = 25) when both extracellular and intracellular genes were considered. This result
467 can again be explained by the fact that UV-induced lesions accumulate most rapidly at TT sites.
468 Consistent with this notion, k values reported for *tetA* (216 and 1200 bp) (Chang et al., 2017)
469 were much lower than the other k values shown in Figure 5a because the *tetA* gene contains
470 fewer TT sites for the same total number of base pairs (Table 1). Third, k values for the gene
471 damage were close to k_{CPDs}. When compared on the basis of total base pairs, the predicted $k_{CPDs\text{-}I}$
472 values exceeded the measured k values by a factor of ~2 when a $\Phi_{CPDs\text{-}I}$ of 2.4×10^{-3} (Görner,
473 1994) was used (Figure 5a) but were similar to the measured k values when a $\Phi_{CPDs\text{-}I}$ of $1.0 \times$
474 10^{-3} (Douki, 2006) was used (Figure S7a). The variation in the CPD quantum yields in literature
475 could be attributed to different analytical methods for quantifying the dimeric photoproducts
476 (e.g., acid hydrolysis, chromatographic separation, and quantification by radioactivity or mass
477 spectrometry) or experimental conditions (e.g., DNA concentration, ionic strength). When
478 compared on the basis of total TT sites, the predicted $k_{CPDs\text{-}II}$ values exceeded the measured k
479 values by a factor of 1.5 (Figure 5b). This level of difference in k (i.e., within a factor of 2) can
480 be considered minor, given the assumptions and uncertainties of the parameters in the k_{CPDs}
481 calculation. Thus, further attempts to improve the kinetic model for $k_{CPDs\text{-}II}$ prediction by
482 considering the photoproducts of bipyrimidine doublets other than TT were not pursued.

Overall, our results indicate that the qPCR method is sensitive enough to detect most major UV-induced DNA damages (e.g., CPDs). This finding is consistent with other studies, which show that the PCR amplification efficiency of genes containing a CPD is drastically reduced (by ~2 $\log_{10}$) compared to the intact gene (Sikorsky et al., 2004).

Enhanced degradation of extracellular ARGs and its impact on elimination of the transforming activity

The kinetic data on the gene damage from this study and from the literature suggest that extracellular genes sometimes undergo more rapid degradation (by a factor of up to 1.7) than the corresponding intracellular genes during UV irradiation (Yoon et al., 2017). This phenomenon was particularly noticeable for some long amplicons (i.e., amp^R and kan^R: 806–851 bp long). The higher reactivity of extracellular genes may have been caused by incidental photochemical reactions of metal–DNA complexes. In particular, photolysis of Cu(II)–DNA complexes has been known to produce Cu(I) and reactive oxygen species (ROS) including $^{\bullet}$OH, which can initiate oxidative DNA damage (Matzeu and Onori, 1986). Even though the plasmid samples in this study were isolated from *E. coli* with a purification step (i.e., washing with phosphate buffer), a certain amount of Cu(II) complexed with DNA could have remained. This explanation can be supported by the observation that the degradation rate of e-amp^R amplicons during UV irradiation of pUC19 decreased by a factor of 1.1–1.7 ($p < 0.05$) after the addition of EDTA (0.1 mM) or methanol (10 mM; Figure S8). EDTA can lower photoreactivity of Cu(II)–DNA complexes by forming a less photoreactive metal–EDTA complex (Natarajan and Endicott, 1973). Methanol can protect DNA by scavenging $^{\bullet}$OH (von Sonntag, 2006). Furthermore, the degradation rate of e-amp^R increased by a factor of ~1.3 ($p < 0.05$) after the addition of $CuSO_4$ (10 μM; Figure S8). Similar photochemical reactions of Cu(II)–DNA complexes could have proceeded and contributed to the enhanced degradation of the

extracellular genes. Nonetheless, this was not the case for the intracellular genes, presumably owing to significant scavenging of UV-induced ROS by intracellular reductants (e.g., sulfur-containing proteins). In agreement with these data, the degradation of extracellular ARGs was significantly enhanced by H_2O_2 addition during UV irradiation of plasmids (Figure 2 and Table 1), whereas no impact of H_2O_2 addition was observed for intracellular ARGs, owing to nearly complete scavenging of $^{\bullet}OH$ by intracellular components (Yoon et al., 2017). These observations may in turn provide an explanation for the relatively poor correlations of measured *k* values with number of base pairs or TT sites for extracellular ARGs in comparison to intracellular ARGs (Figure 5).

It is noteworthy that the enhanced degradation of extracellular ARGs beyond the direct UV-induced damage does not lead to more rapid elimination of the transforming activity. The rate of elimination of transforming activity was nearly constant across the UV and UV/H_2O_2 treatments of e-ARGs, while the gene degradation rates varied by a factor of up to 1.8 ($p < 0.05$) for the same treatments (Figure 2 and Table 1). Thus, the damage to extracellular ARGs by UV, $^{\bullet}OH$, or other ROS was detectable by the qPCR method, but in the *E. coli* transformation assay, only the direct UV-induced gene damage could be detected. This finding could be due to efficient repair of the gene damage caused by $^{\bullet}OH$ (or other ROS) in the *E. coli* transformation system. Single oxidized bases (e.g., 5,6-dihydroxy-5,6-dihydrothymine) are the most frequent type of nucleobase damage in cellular DNA from exposure to $^{\bullet}OH$, and most such lesions are efficiently removed by the cellular base excision repair system (Cadet and Wagner, 2013). Such DNA repair function does not exist in the qPCR system. In addition to the DNA repair, the difference in fidelity between *E. coli* DNA polymerase and *Taq* DNA polymerase could have played a role. *E. coli* is known to possess specialized lesion bypass DNA polymerases with low fidelity that enable translesion replication of damaged DNA (Maor-Shoshani et al., 2003; Nevin et al., 2017). In contrast, *Taq* polymerase of the qPCR method is a relatively high-fidelity

polymerase with high enough sensitivity to detect even minor single-base lesions (Sikorsky et al., 2004).

Conclusions

- Under typical UV fluences for disinfection purposes (e.g., 40 mJ/cm^2), a ~1 log reduction in the transforming activity of a plasmid-encoded ARG is expected. To achieve more extensive elimination of the transforming activity (e.g., >4 log reduction), UV fluence of more than 150 mJ/cm^2 is required. Addition of H_2O_2 (i.e., the UV/H_2O_2 advanced oxidation process) does not significantly enhance the efficiency of elimination of the transforming activity.
- Efficiency of elimination of the transforming activity for a plasmid-encoded ARG during UV treatment depends on the rate of formation of CPDs in the plasmid and the repair of such DNA damage during the transformation process in host cells. Significant capacity for CPD repair is present in the *E. coli* recipient strain (DH5α) used in this study and is also expected in many wild-type bacterial cells.
- The rate of formation of CPDs can be calculated by considering the number of TT sites in target gene fragments or whole plasmids and the TT-specific photochemical reaction parameters (i.e., $\Phi_{CPD,TT} = 2.0 \times 10^{-2}$ and $\varepsilon_{TT} = 8{,}400$ M^{-1} cm^{-1} for 254 nm light). Additionally, CPDs can be sensitively detected and quantified by qPCR.
- CPD formation is the major DNA damage mechanism and responsible for the elimination of transforming activity of extra- and intracellular plasmids during UV and UV/H_2O_2 treatment.
- For extracellular plasmids, DNA base oxidation takes place in addition to CPD formation, and these lesions are detectable by the qPCR method. The DNA base oxidation, however, does not reduce the transforming activity of pUC19 in the *E. coli* recipient strain (DH5α) utilized here.

Supporting Information

Three texts, two tables, and eight figures are available as supplementary materials and data.

Acknowledgements

This study was supported by the National Research Foundation funded by the Ministry of Science, ICT & Future Planning (NRF-2017R1A2B2002593) and the Korea Environmental Industry & Technology Institue (KEITI-2015001800001). Additional support for MCD from U.S. National Science Foundation Award CBET-1254929 is gratefully acknowledged.

References

Alexander, J., Knopp, G., Dötsch, A.,Wieland, A., Schwartz, T., 2016. Ozone treatment of conditioned wastewater selects antibiotic resistance genes, opportunistic bacteria, and induce strong population shifts. Sci. Total. Environ. 559, 103-112.

Allen et al., 2010, Call of the wild: antibiotic resistance genes in natural environments. Nature Rev. 8, 251-259.

Berendonk, T., Manaia, C.M., Merlin, C., Fatta-Kassinos, D., Cytryn, E., Walsh, F., Bürgmann, H., Sørum, H., Norström, M., Pons, M.-N., Kreuzinger, N., Huovinen, P., Stefani, S., Schwartz, T., Kisand, V., Baquero, F., Martinez, J.L., 2015. Tackling antibiotic resistance: the environmental framework. Nature reviews Microbiol. 13, 310–317.

Bioneer, *AccuPrep*® Nano-Plus Plasmid Mini/Midi/Maxi Extraction Kit, User's Guide. Korea, 2016. Available at http://us.bioneer.com/Protocol/AccuPrep%20Nano-Plus%20Plasmid%20Extraction%20Kit.pdf.

Bolton, J.R., Linden, K.G., 2003, Standardization of methods for fluence (UV dose)

579 determination in bench-scale UV experiments, J. Environ. Eng., 129, 209–215.
580 Cadet, J., Wagner, J.R., 2013, DNA base damage by reactive oxygen species, oxidizing agents,
581 and UV radiation. Cold Spring Harb Perspect Biol. 5, a012599.
582 Cadet, J., Douki, T., Formation of UV-induced DNA damage contributing to skin cancer
583 development, Photochem. Photobiol. Sci., 2018.
584 Casali, N., Preston, A. *E. coli Plasmid Vectors. Methods and Applications*. Humana Press Inc.,
585 New York, Springer, 2003.
586 Chang et al., Degradation of Extracellular Antibiotic Resistance Genes with UV_{254} Treatment,
587 Environ. Sci. Technol., 2017, 51, 6185-6192.
588 Chen, H., Zhang, M., 2013. Effects of advanced treatment systems on the removal of antibiotic
589 resistance genes in wastewater treatment plants from Hangzhou, China. Environ. Sci.
590 Technol. 47, 8157-8163.
591 Colomer-Lluch, M., Jofre, J., Muniesa, M., 2011. Antibiotic resistance genes in the
592 bacteriophage DNA fraction of environmental samples, PloS One, 6, e17549.
593 Czekalski, N., Berthold, T., Caucci, S., Egli, A., Bürgmann, H., 2012. Increased levels of
594 multiresistant bacteria and resistance genes after wastewater treatment and their
595 dissemination into Lake Geneva, Switzerland. Front. Microbiol. 3, 1-18.
596 Destiani, R., Templeton, M.R., Kowalski, W., 2017. Relative ultraviolet sensitivity of selected
597 antibiotic resistance genes in waterborne bacteria. Environ. Eng. Sci. In press.
598 https://doi.org/10.1089/ees.2017.0179.
599 Dodd, M.C., 2012. Potential impacts of disinfection processes on elimination and deactivation
600 of antibiotic resistance genes during water and wastewater treatment. J. Environ. Monit. 14,
601 1754–1771.
602 Douki, T., Cadet J., Individual determination of the yield of the main UV-induced dimeric
603 pyrimidine photoproducts in DNA suggests a high mutagenicity of CC photolesions,

Biochemistry 2001, 40, 2495-2501.

Douki, T. Low ionic strength reduces cytosine photoreactivity in UVC-irradiated isolated DNA, Photochem. Photobiol. Sci. 2006, 5, 1045-1051.

Ferro, G., Guarino, F., Cicatelli, A., Rizzo, L., 2017. β-lactams resistance gene quantification in an antibiotic resistant *Escherichia coli* water suspension treated by advanced oxidation with UV/H_2O_2. J. Hazard. Mater. 323, 426-433.

Gerrity, D., et al 2016. Emerging investigators series: prediction of trace organic contaminant abatement with UV/H_2O_2: development and validation of semi-empirical models for municipal wastewater effluents, Environ. Sci.: Water Res, 2, 460-473.

Görner, H., Photochemistry of DNA and related biomolecules: quantum yields and consequences of photoionization. J. Photochem. Photobiol. B. Biology, 1994, 26, 117–139.

Gurzadyan, G.G., Görner, H., Schulte-Frohlinde, D., Photolesions and biological inactivation of plasmid DNA on 254nm irradiation and comparison with 193nm laser irradiation, Photochem. Photobiol., 1993, 58, 477-485.

Hanahan D, 1983, Studies on transformation of *Escherichia coli* with plasmids. J. Mol. Biol., 166, 557-580.

Hanahan, D., Jessee, J., Bloom, F.R., Plasmid transformation of *Escherichia coli* and other bacteria. Methods in Enzymology, 1991, 204, 63-113.

Jacangelo, J.G., Trussell, R.R., 2002. International report: water and wastewater disinfection-trends, issues, and practices. Water Sci. Technol. Water Supply 2, 147-157.

Kisker, C., Kuper, J., van Houten, B., Prokaryotic nucleotide excision repair, Cold Spring Harb Perspect Biol, 2013, 5, a012591.

Lee, Y., Gerrity, D., Lee, M., Gamage, S., Pisarenko, A., Trenholm, R.A., Canonica, S., Snyder, S.A., von Gunten, U., 2016. Organic contaminant abatement in reclaimed water by UV/H_2O_2 and a combined process consisting of O_3/H_2O_2 followed by UV/H_2O_2: prediction

629 of abatement efficiency, energy consumption, and byproduct formation. Environ Sci
630 Technol, 50, 3809−3819.
631 Lee, Y., von Gunten, U., 2016. Advances in predicting organic contaminant abatement during
632 ozonation of municipal wastewater effluent: reaction kinetics, transformation products, and
633 changes of biological effects, Environ. Sci.: Water Res, 2, 421-442.
634 Luby, E., Ibekwe, A.M., Zilles, J., Pruden, A., 2016. Molecular methods for assessment of
635 antibiotic resistance in agricultural ecosystems: prospects and challenges. J. Environ.
636 Quality 45, 441-453.
637 Lüddeke, F., Heb, S., Gallert, C., Winter, J., Güde, H., Löffler, H., 2015. Removal of total and
638 antibiotic resistant bacteria in advanced wastewater treatment by ozonation in combination
639 with different filtering techniques. Water Res. 69, 243-251.
640 Lusetti, S.L., Cox, M.M., The bacterial RecA protein and the recombinational DNA repair of
641 stalled replication forks, Annual Rev. Biochem. 2002, 71, 71-100.
642 Maor-Shoshani, A., Ben-Ari, V., Livneh, Z., 2003. Lesion bypass DNA polymerase replicate
643 across non-DNA segments. PNAS, 100, 14760-14765.
644 Matzeu, M., Onori, G., 1986. Effect of mid-UV radiation on DNA-Cu^{2+} complex: absorption
645 and circular dichroism study. Photochem. Photobiol. 44, 59-65.
646 Mouret, S., Charveron, M., Favier, A., Cadet, J., & Douki, T., 2008. Differential repair of UVB-
647 induced cyclobutane pyrimidine dimers in cultured human skin cells and whole human
648 skin. DNA repair, 7(5), 704-712.
649 McKinney, C.W., Pruden, A., 2012. Ultraviolet disinfection of antibiotic resistant bacteria and
650 their antibiotic resistance genes in water and wastewater. Environ. Sci. Technol, 46,
651 13393−13400.
652 Miklos, D.B., Hartl, R., Michel, P., Linden, K.G., Drewes, J.E., Hübner, U., 2018. UV/H_2O_2
653 process stability and pilot-scale validation for trace organic chemical removal from

654 wastewater treatment plant effluents. Water Res, in press.
655 Natarajan, P., Endicott, J.F., 1973. Photoredox behavior of transition metal-
656 ethylenediaminetetraacetate complexes. A comparison of some group VII metals. J. Phys.
657 Chem. 77, 2049-2054.
658 Nevin, P., Gabbai, C.C., Marians, K.J., 2017. Replisome-mediated translesion synthesis by a
659 cellular replicase. J. Biol. Chem. 292, 13833-13842.
660 Palmen et al., Physiological characterization of natural transformation in *Acinetobacter*
661 *calcoaceticus*, J. General Microbiol, 1993, 139, 295-305.
662 Pak, G., Salcedo, D. E., Lee, H., Oh, J., Maeng, S. K., Song, K. G., Hong, S. W., Kim, H.-C.,
663 Chandran, K., Kim, S., 2016. Comparison of antibiotic resistance removal efficiencies using
664 ozone disinfection under different pH and suspended solids and humic substance
665 concentrations. Environ. Sci. Technol. 50, 7590−7600.
666 Patrick, M.H., 1977. Studies on thymine-derived UV photoproducts in DNA-I. Formation and
667 biological role of pyrimidine adducts in DNA. Photochem. Photobiol. 25, 357-372.
668 Pingound, A., Jeltsch, A., Structure and function of type II restriction endonucleases, Nucleic
669 Acids Research, 2001, 29, 3705-3727.
670 Pruden, A., 2014. Balancing water sustainability and public health goals in the face of growing
671 concerns about antibiotic resistance. Environ. Sci. Technol. 48, 5–14.
672 Rizzo, L., Manaia, C., Merlin, C., Schwartz, T., Dagot, C., Poly, M.C., Michael, I., Fatta-
673 Kassinos, D., 2013. Urban wastewater treatment plants as hotspots for antibiotic resistant
674 bacteria and genes spread into the environment: a review. Sci. Total. Environ. 447, 345e360.
675 Shanehbandi D, Saei AA, Zarredar H, Barzegari A., Vibration and glycerol-mediated plasmid
676 DNA transformation for Escherichia coli, FEMS Microbiol Lett, 2013, 348, 74–78
677 Schneider, C. A., Rasband, W. S., & Eliceiri, K. W., 2012, NIH Image to ImageJ: 25 years of
678 image analysis, Nature methods, 9, 671-675.

679 Schulte-Frohlinde, D., Biological consequences of strand breaks in plasmid and viral DNA, Br.
680 J. Cancer, 1987, 55, 129-134.
681 Sikorsky, J.A., Primerano, D.A., Fenger, T.W., Denvir, J., Effect of DNA damage on PCR
682 amplification efficiency with the relative threshold cycle method, BBRC, 2004, 323, 823-
683 830.
684 Sinha, R.P., Häder, D.-P., UV-induced DNA damage and repair: a review, Photochem.
685 Photobiol. Sci., 2002, 1, 225-236.
686 Sousaa, J.M., Macedob, G., Pedrosac, M., Becerra-Castroa, C., Castro-Silvad, S., Pereirac,
687 M.F.R., Silva, A.M.T., Nunesa, O.C., Manaia, C.M., 2017. Ozonation and UV254nm
688 radiation for the removal of microorganisms and antibiotic resistance genes from urban
689 wastewater. J. Hazard. Mater. 323, 434-441.
690 Tan, D.T., Shuai, D., 2015. Research highlights: antibiotic resistance genes: from wastewater
691 into the environment. Environ. Sci.: Water Res, 1, 264-267.
692 Tataurov, A.V., You, Y., Owczarzy, R., 2008. Predicting ultraviolet spectrum of single stranded
693 and double stranded deoxyribonucleic acids. Biophys. Chem. 133, 66–70.
694 Thomas, C.M., Nielsen, K.M., 2005. Mechanisms of, and barriers to, horizontal gene transfer
695 between bacteria, Nature Reviews Microbiology 3, 711-721.
696 Vikesland, P.J., et al., 2017. Toward a comprehensive strategy to mitigate dissemination of
697 environmental sources of antibiotic resistance, Environ. Sci. Technol., 51, 13061-13069.
698 Von Sonntag, C., 2006. Free-radical-induced DNA Damage and its Repair. A Chemical
699 Perspective. Springer Verlang, Heidelberg, Berlin.
700 World Health Organization, 2014. Antimicrobial Resistance: Global Report on Suveillance.
701 WHO.
702 Yoon et al., 2017. Inactivation efficiency of plasmid-encoded antibiotic resistance genes during
703 water treatment with chlorine, UV, and UV/H_2O_2, Water Res, 123, 783-793.

704 Zhang, Y., et al., 2018. Cell-free DNA: A neglected source for antibiotic resistance genes
705 spreading from WWTPs. Environ. Sci. Technol. 52, 248-257.

Table 1. Fluence-based rate constants (k_{CPD-I} and k_{CPD-II}) for gene damage quantified by qPCR during treatment of intracellular and extracellular plasmids with UV and UV/H_2O_2.

Gene	#base pairs [a]	#TT sites [b]	Plasmid location	k, cm^2/mJ [c]	k_{CPDs} (bps), cm^2/mJ [d]	k_{CPDs} (TTs), cm^2/mJ [e]	Ref. [f]
UV treatment							
amp^R (pUC19)	192	42	Intra	$1.7(\pm0.09)\times10^{-2}$	3.4×10^{-2}	3.4×10^{-2}	This study
			Extra	$1.9(\pm0.11)\times10^{-2}$			
	400	67	Intra	$2.8(\pm0.06)\times10^{-2}$	7.0×10^{-2}	5.5×10^{-2}	
			Extra	$3.1(\pm0.09)\times10^{-2}$			
	603	96	Intra	$4.6(\pm0.18)\times10^{-2}$	1.1×10^{-1}	7.9×10^{-2}	
			Extra	$5.4(\pm0.16)\times10^{-2}$			
	851	118	Intra	$7.2(\pm0.35)\times10^{-2}$	1.5×10^{-1}	9.7×10^{-2}	
			Extra	$1.0(\pm0.03)\times10^{-1}$			
ori (pUC19)	190	29	Extra	$1.7(\pm0.09)\times10^{-2}$	3.3×10^{-2}	2.4×10^{-2}	This study
	390	44	Extra	$2.9(\pm0.12)\times10^{-2}$	6.9×10^{-2}	3.6×10^{-2}	
	530	59	Extra	$4.0(\pm0.24)\times10^{-2}$	9.3×10^{-2}	4.8×10^{-2}	
amp^R (pUC4k)	850	119	Intra	6.8×10^{-2}	1.5×10^{-1}	9.8×10^{-2}	Yoon et al, 2017
			Extra	1.1×10^{-1}			
kan^R (pUC4k)	806	134	Intra	8.1×10^{-2}	1.4×10^{-1}	1.1×10^{-1}	Yoon et al, 2017
			Extra	1.4×10^{-1}			
bla$_{TEM-1}$	209	30	Extra	5.5×10^{-3}	3.7×10^{-2}	2.5×10^{-2}	Chang et al, 2017
	861	123	Extra	6.8×10^{-2}	1.5×10^{-1}	1.0×10^{-1}	
tetA	216	18	Extra	3.8×10^{-2}	3.8×10^{-2}	1.5×10^{-2}	Chang et al, 2017
	1200	80	Extra	5.8×10^{-2}	2.1×10^{-1}	6.6×10^{-2}	
UV/H_2O_2 treatment							
amp^R (pUC19)	192	42	Intra	$1.6(\pm0.09)\times10^{-2}$	3.4×10^{-2}	3.4×10^{-2}	This study
			Extra	$2.5(\pm0.14)\times10^{-2}$			
	400	67	Intra	$2.9(\pm0.12)\times10^{-2}$	7.0×10^{-2}	5.5×10^{-2}	
			Extra	$4.1(\pm0.16)\times10^{-2}$			
	603	96	Intra	$4.8(\pm0.28)\times10^{-2}$	1.1×10^{-1}	7.9×10^{-2}	
			Extra	$6.7(\pm0.28)\times10^{-2}$			
	851	118	Intra	$7.3(\pm0.30)\times10^{-2}$	1.5×10^{-1}	9.7×10^{-2}	
			Extra	$1.8(\pm0.06)\times10^{-1}$			
ori (pUC19)	190	29	Extra	$2.3(\pm0.05)\times10^{-2}$	3.3×10^{-2}	2.4×10^{-2}	This study
	390	44	Extra	$3.9(\pm0.14)\times10^{-2}$	6.9×10^{-2}	3.6×10^{-2}	
	530	59	Extra	$4.7(\pm0.21)\times10^{-2}$	9.3×10^{-2}	4.8×10^{-2}	
amp^R	850	119	Intra	6.7×10^{-2}	1.5×10^{-1}	9.8×10^{-2}	Yoon

(pUC4k)			Extra	1.7×10^{-1}			et al, 2017
kan^{R} (pUC4k)	806	134	Intra	8.0×10^{-2}	1.4×10^{-1}	1.1×10^{-1}	Yoon et al, 2017
			Extra	2.5×10^{-1}			

[a]Total number of base pairs, [b]Total number of TT sites, [c]Fluence-based rate constant measured from this study and literature, [d]Fluence-based rate constant for CPD formation calculated using k_{CPDs} = (2.303 × ε_{bp} × $\Phi_{CPD,I}$) / U, ε_{bp} = ε_{sbp} × (#base pair) = (15,000 M^{-1} cm^{-1}) × (#base pair), and $\Phi_{CPD,I}$ = 2.4×10^{-3} (Gorner, 1994), [e]Calculated using k_{CPDs} = (2.303 × ε_{TT} × $\Phi_{CPD,TT\text{-}II}$) / U, ε_{TT} = $\varepsilon_{sTT,254}$ × (#TT) = (8,400 M^{-1} cm^{-1}) × (#TT), and $\Phi_{CPD,TT\text{-}II}$ = 2.0×10^{-2} (Douki et al., 2000), [f]Source for the measured *k* values.

Table 2. Fluence-based rate constants ($k_{CPD\text{-}I}$ and $k_{CPD\text{-}II}$) for the elimination of transforming activity of ARGs during UV treatment of extracellular plasmids.

Plasmid	**#base pairs** [a]	**#TT sites** [b]	**Host cell for transformation**	***k*, cm^2/mJ** [c]	**k_{CPDs} (bps), cm^2/mJ** [d]	**k_{CPDs} (TTs), cm^2/mJ** [e]	**Ref.** [f]
pUC19	2686	383	*E. coli* DH5α (recA$^-$)	6.1×10^{-2}	4.7×10^{-1}	3.1×10^{-1}	This study
pTZ18R	2861	453	*E. coli* K12 AB2480 (uvrA$^-$, recA$^-$)	5.3×10^{-1}	5.0×10^{-1}	3.7×10^{-1}	Gurzadyan et al, 1993
			E. coli K12 AB1886 (uvrA$^-$)	7.1×10^{-2}			
			E. coli K12 AB2463 (recA$^-$)	6.7×10^{-2}			
			E. coli K12 AB1157 (wild type)	2.4×10^{-2}			
pBR322	4361	513	*E. coli* K12 AB2480 (uvrA$^-$, recA$^-$)	6.7×10^{-1}	7.7×10^{-1}	4.2×10^{-1}	Gurzadyan et al, 1993
			E. coli K12 AB1157 (wild type)	4.4×10^{-2}			
pWH1266	8890	- [g]	*Acinetobacter baylyi*	1.1×10^{-1}	1.56	- [g]	Chang et al, 2017

[a]Total number of base pairs, [b]Total number of TT sites, [c]Fluence-based rate constant measured from this study and literature, [d]Fluence-based rate constant for CPD formation calculated using $k_{CPDs} = (2.303 \times \varepsilon_{bp} \times \Phi_{CPD,I}) / U$, $\varepsilon_{bp} = \varepsilon_{sbp} \times$ (#base pair) = (15,000 M^{-1} cm^{-1}) × (#base pair), and $\Phi_{CPD,I} = 2.4\times10^{-3}$ (Gorner, 1994), [e]Calculated using $k_{CPDs} = (2.303 \times \varepsilon_{TT} \times \Phi_{CPD,TT\text{-}II}) / U$, $\varepsilon_{TT} = \varepsilon_{sTT,254} \times$ (#TT) = (8,400 M^{-1} cm^{-1}) × (#TT), and $\Phi_{CPD,TT\text{-}II} = 2.0\times10^{-2}$ (Douki et al., 2000) [f]Source for the measured *k* values, [g]Not available because the full gene sequence is not known.

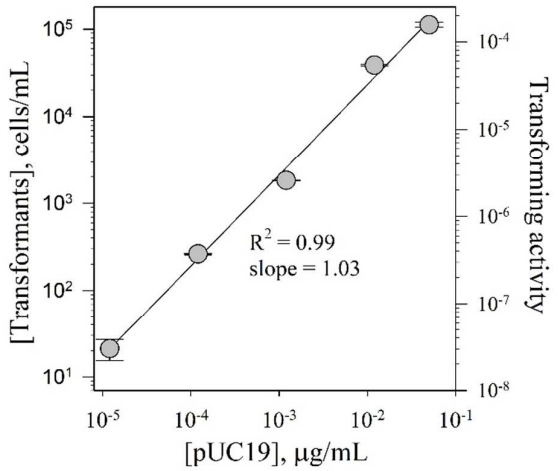

Figure 1. Concentration of transformants and resulting transforming activity as a function of pUC19 concentration during transformation of *amp*^{R} to *E. coli* DH5α. The error bars represent one-standard deviation of more than three replicate measurements.

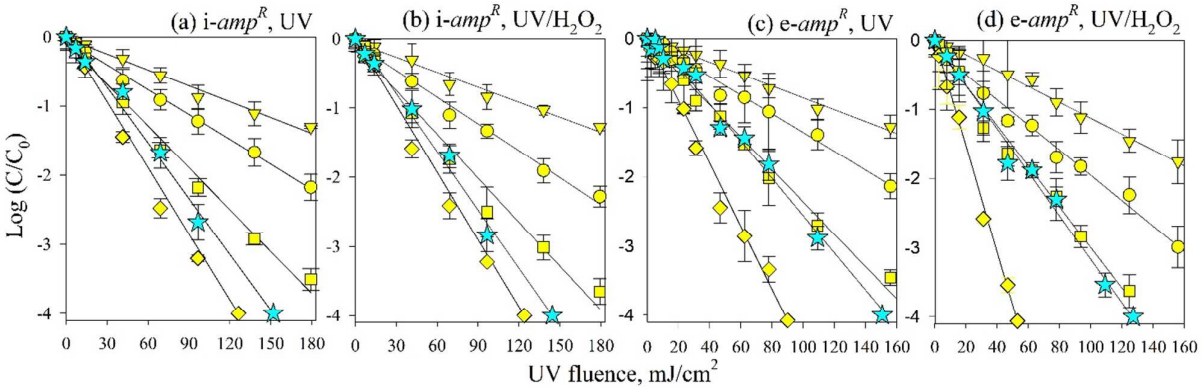

Figure 2. Logarithmic relative concentration of the transforming activity (★) and *amp*^{R} qPCR amplicons (192 bps (▽), 400 bps (○), 603 bps (□) and 851 bps (◇)) as a function of UV fluence during treatment of (a, b) intracellular and (c, d) extracellular pUC19 with (a, c) UV and (b, d) UV/H_2O_2 ($[H_2O_2]_0$ = 10 mg/L) at pH 7. The symbols represent the measured data and the error bars represent one standard deviation from triplicate experiments. The lines are linear regressions of the data.

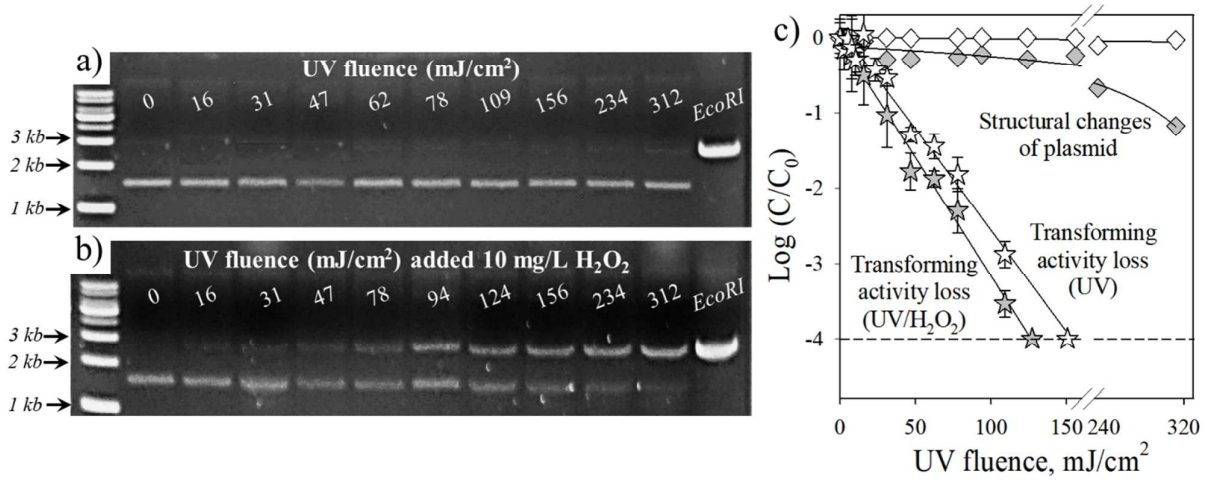

Figure 3. Agarose gel electrophoresis images of extracellular pUC19 plasmids treated with (a) UV and (b) UV/H_2O_2 ($[H_2O_2]_0$ = 10 mg/L) as a function of UV fluence (0 – 312 mJ/cm^2). The first column shows gel images of standard ladders. The last column shows gel images of the pUC19 plasmid treated by restriction enzyme (*EcoRI*). (c) Logarithmic-scale decreases of the structural integrity (from quantitative analysis of the electrophoresis images) and transforming activity of pUC19 as a function of UV fluence.

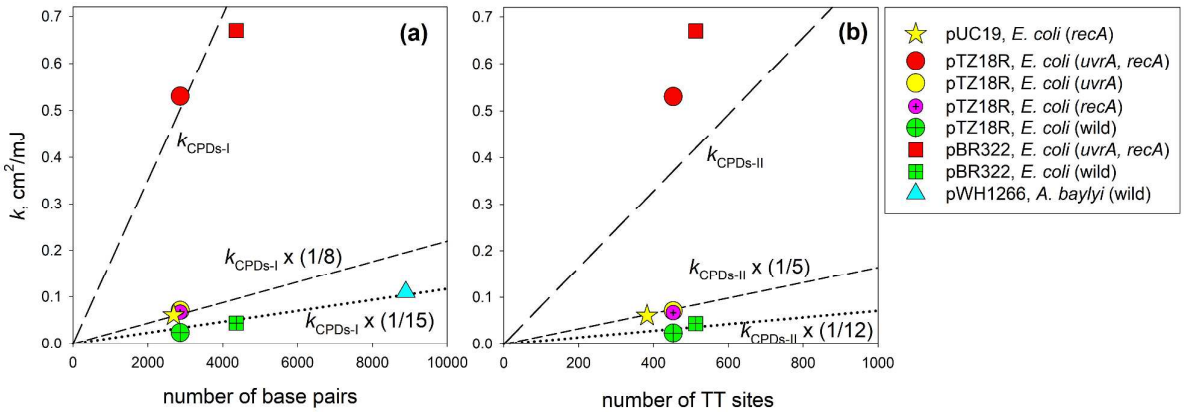

Figure 4. UV fluence-based rate constants (k) for elimination of transforming activity of plasmids as a function of number of (a) base pairs (k_{CPDs-I}) and (b) TT sites ($k_{CPDs-II}$). The k data were obtained from this study (pUC19) and taken from Gurzadyan et al, 1993 (pTZ18r and pBR322), and Chang et al, 2017 (pWH1266) (see Table 2). The long-dash lines indicate the rate constants calculated for CPD formation across the entire plasmid (k_{CPDs}). For (a), a Φ_{CPDs-I} value of 2.4×10^{-3} (Görner, 1994) was used to calculate the k_{CPDs-I} for the photons absorbed by entire DNA. For (b), a $\Phi_{CPDs-TT}$ value of 2.0×10^{-2} (Douki et al., 2000) was used to calculate the $k_{CPDs-II}$ for the photons absorbed by all TT sites within entire DNA. The short-dash and dotted lines are the k_{CPDs} multiplied with slope factors (ranging from 1/15 to 1/5) that were obtained to fit the measured k values. See the main text for further explanation.

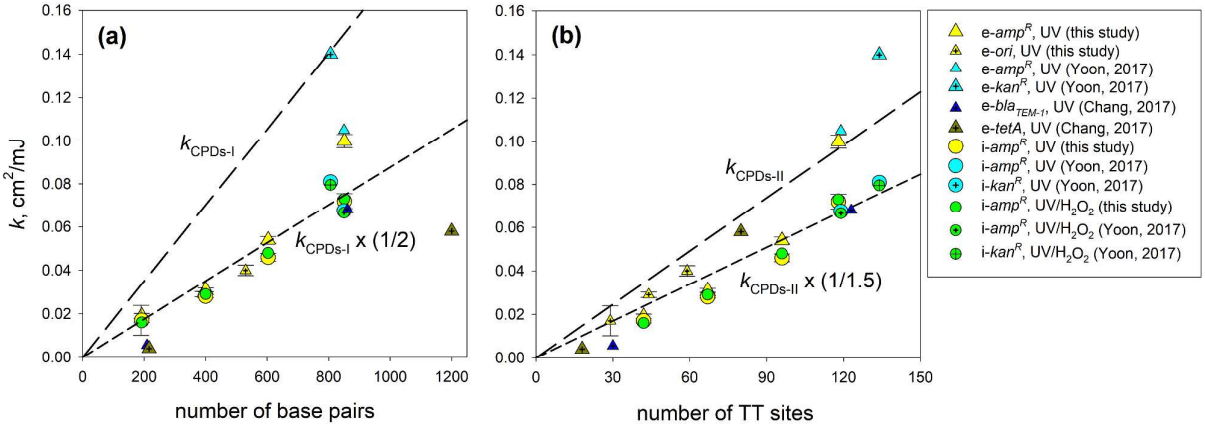

Figure 5. UV fluence-based rate constants (k) for gene damage of extracellular (e-ARGs, triangles) and intracellular (i-ARGs, circles) plasmid-encoded genes as a function of number of (a) base pairs (k_{CPD-I}) and (b) TT sites (k_{CPD-II}). The k data were obtained from this study, and taken from Yoon et al., 2017, and Chang et al., 2017 (see Table 1). The long-dash lines indicate the calculated rate constant for the CPD formation (k_{CPDs}). For (a), a Φ_{CPDs-I} value of 2.4×10^{-3} (Görner, 1994) was used, and for (b), a $\Phi_{CPDs-TT}$ value of 2.0×10^{-2} (Douki et al., 2000) was used. The short-dash lines are linear regressions of the k values of intracellular genes in which the relative slope of k compared to k_{CPDs} are indicated. See Figure 4 and the main text for further explanation.

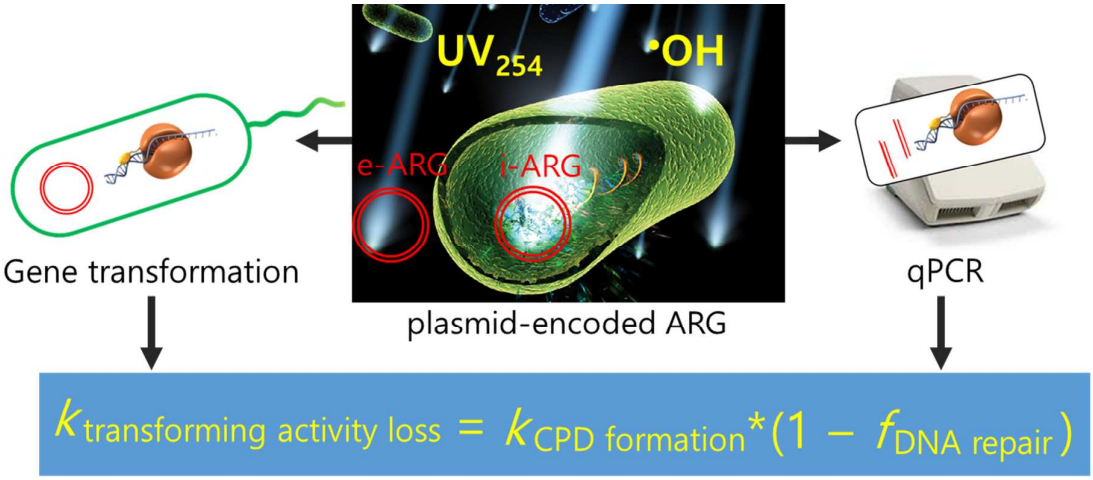

$$k_{\text{transforming activity loss}} = k_{\text{CPD formation}} * (1 - f_{\text{DNA repair}})$$